Archives of Oral Biology 76 (2017) 20–29

Contents lists available at ScienceDirect

Archives of Oral Biology

journal homepage: www.elsevier.com/locate/aob

Time dependent deformation behavior of dentin

C. Montoya[a], D. Arola[b,c], E.A. Ossa[a,*]

[a] School of Engineering, Universidad Eafit, Medellín, Colombia
[b] Department of Materials Science & Engineering, University of Washington, Seattle, WA, USA
[c] Departments of Restorative Dentistry and Oral Health Sciences, School of Dentistry, University of Washington, Seattle, WA, USA

ARTICLE INFO

Article history:
Received 21 September 2016
Received in revised form 15 November 2016
Accepted 3 January 2017

Keywords:
Dentin
Spherical indentation
Creep
Mineral-to-collagen ratio
Lumen area fraction

ABSTRACT

Objective: The viscoelastic behavior of dentin and its ability to undergo time dependent deformation are considered to be important to oral functions and its capacity to resist fracture. There are spatial variations in the microstructure of dentin within the crown, which could be important to the viscous behavior. However, a spatially resolved description for the viscoelastic behavior of coronal dentin has not been reported.
Methods: In this investigation spherical indentations were made in three regions of coronal dentin including the outer, middle and inner regions. Power law relations were developed to quantitatively describe the stress-strain responses of the tissue.
Results: Results showed that the deformation behavior was strongly dependent on the composition (mineral to collagen ratio) and microstructure (tubule density), which contributed to an increase in the rate of viscous deformation with increasing proximity to the pulp.
Conclusions: A model accounting for spatial variations in composition and microstructure was developed to describe the steady-state time dependent deformation behavior of coronal dentin, and a good agreement was found with the experimental results.

1. Introduction

Most biological tissues exhibit viscoelastic behavior, which is considered to be important to their function. For instance, the time dependent deformation behavior of dentin potentially contributes to the distribution of loads within the tooth and the resistance to fracture (Duncanson & Korostoff, 1975; Kinney, Marshall, & Marshall, 2003; Trengrove, Carter, & Hood, 1995).

The mechanical response of dentin results from the interaction between the organic and mineral constituents. Dentin consists of approximately 45% mineral, 33% organic material (collagen type I) and 22% water by volume (Nanci, 2008). Although this chemical composition is assumed for the tissue overall, it has been widely recognized that these percentages change spatially within the tooth (Montoya, Arango-Santander, Peláez-Vargas, Arola, & Ossa, 2015; Ryou et al., 2011; Tesch et al., 2001; Xu, Yao, Walker, & Wang, 2009). The combination of hard mineral crystals (i.e. hydroxyapatite) and highly viscous organic material (i.e. collagen) results in a viscoelastic material with time dependent behavior (Deymier-Black et al., 2012; Kinney et al., 2003; Shen, Kahn, Ballarini, & Eppell, 2011). Microscopic evaluations of the microstructure are dominated by the dentinal tubules, which are a network of small (diameter of approx. 1 μm) canals that traverse the entire thickness of dentin. The tubule density ranges from 20,000 to 55,000 tubules/mm^2 and may function hydraulically during stress transfer (Nanci, 2008; Pashley, Okabe, & Parham, 1985).

The mechanical properties of dentin have been extensively investigated in response to quasi-static tension, bending and shear loading. A comprehensive review of these studies was reported by Kinney et al. (2003). Few studies have analyzed the time dependent behavior of dentin. For instance, Korostoff, Pollack, & Duncanson (1975) analyzed the viscoelastic behavior of radicular dentin under compressive loads, finding that the relaxation modulus exhibited a linear dependence on the logarithm of time. The mathematical model of viscoelasticity previously presented by Alfrey and Doty (1945) was compared with their experimental results and suggested that the stress relaxation response of dentin follows a linear viscoelastic behavior. However, due to the differences in microstructure between the crown and root (Arola et al., 2009), it is not clear if this behavior can be extrapolated to coronal dentin. On the other hand, Jafarzadeh, Erfan, and Watts (2004) evaluated coronal dentin under two different compressive stresses and temperatures and reported linear viscoelastic behavior. Nevertheless, the spatial variations in microstructure

* Corresponding author at: School of Engineering, Universidad Eafit, Cra 49 No 7 sur 50, Medellín, Colombia.
E-mail address: eossa@eafit.edu.co (E.A. Ossa).

http://dx.doi.org/10.1016/j.archoralbio.2017.01.003
0003-9969/

and tubules were not considered, which could contribute to the time dependent behavior of this tissue.

Using nano-Dynamic Mechanical Analysis (DMA), Ryou, Romberg, Pashley, Tay, and Arola (2012) studied the viscoelastic behavior of peritubular and intertubular dentin separately. Indentations were made with a dynamic load amplitude of 20 μN, and over frequencies varying from 2 to 100 Hz. The dynamic mechanical properties increased in magnitude with loading frequency. Interestingly, although the complex and storage moduli of peritubular dentin were significantly larger than those for intertubular dentin, there were no significant differences in the loss modulus and $tan\delta$ between the intertubular and peritubular dentin. Recently, Chuang et al. (2015) performed nanoindentation creep tests to study the viscoelastic properties of dentin after de- and re-mineralization processes. Demineralization increased the primary and secondary creep regimes, whereas remineralization reduced the primary creep response of dentin without changes to the viscoelastic behavior. Additional creep tests on dentin have also been reported (Han et al., 2012; Bertassoni, Kury, Rathsam, Little, & Swain, 2015).

Indentation techniques have been widely used to analyze the viscoelastic properties of tissues and biological materials (i.e. bone and teeth) (Staines, Robinson, & Hood, 1981; Ahearne, Yang, Then, & Liu, 2007; Cheneler, Mehrban, & Bowen, 2013). Indentation is an attractive method due to its ability to obtain reliable results without causing substantial damage to the tissue. Of course, there is permanent deformation to the sample, which is a function of indenter shape and load. Various types of indenters have been used for these tests such as spherical, conical and pyramidal. Sharp indenters introduce a discontinuity at the tip followed by immediate inelasticity, while spherical indenters produce a uniform and axisymmetric distribution of stresses, allowing a soft transition between elastic and viscoelastic regimes during the indenter penetration, simplifying the viscoelastic behavior analysis of the material (Bower, Fleck, Needleman, & Ogbonna, 1993; Kim, 2008).

Despite these previous studies for the viscoelastic properties of dentin, little is known about its time-dependent deformation and the effect of spatial variations within the crown. During mastication coronal dentin is subjected to a variety of cyclic stresses in which the viscoelastic response of the tissue could deter crack initiation, and increase the resistance to fracture. Understanding the time-dependent loading deformation behavior of coronal dentin and the contribution of spatial variations in microstructure is important to understand the structural behavior of teeth and in the development of new dental materials with mechanical properties consistent with those of the hard tissue. Therefore, the aim of this work was to develop a simple model for the time dependent loading deformation behavior of coronal dentin in the steady-state regime (or secondary creep), considering the spatial variations in microstructure and composition within dentin. First, an experimental study of the spherical indentation behavior of coronal dentin is presented. Based on the experimental results, a model based on previously proposed theories for indentation of time dependent materials is proposed and validated.

2. Background

Several models have been proposed to determine the displacement and stress fields produced in a time dependent material under a rigid indenter (e.g. Bower et al., 1993; Graham, 1965; Hunter, 1960; Lee and Radok, 1960). Bower et al. (1993) solved the problem of axisymmetric indentation of a half-space comprised of a power-law creep material of the form:

$$\dot{\varepsilon} = \dot{\varepsilon}_o \left(\frac{\sigma}{\sigma_o}\right)^n, \tag{1}$$

using the similarity transformations suggested by Hill, Storakers, and Zdunek (1989), where σ_o and $\dot{\varepsilon}_o$ are the reference stress and strain rates, and n the power law creep exponent of the material. These transformations are based on the observation that at any given instant, the velocity, strain rate and stress fields in the half-space only depend on the size of the contact a and the indentation rate $\dot{h}$, and are independent of the loading history (see Fig. 1). Thus, the general indentation problem is reduced to calculating stresses and displacements in a non-linear elastic solid, indented to a unit depth by a rigid flat punch of unit radius (in the axisymmetric problem). For indentation by a frictionless spherical indenter, the similarity solutions dictate that the contact radius a is related to the indentation depth h by:

$$a = c\sqrt{2Rh}, \tag{2}$$

where a is the contact radius and R is the radius of the indenter. The constant c is only a function of the material creep exponent n and may be thought of as the ratio of the true to nominal contact radius, where the nominal contact radius is $\sqrt{2Rh}$. Similarly, the applied load F is related to the indentation rate $\dot{h}$ via:

$$\frac{F}{\pi a^2 \sigma_o} = \alpha\left(\frac{\dot{h}}{a\dot{\varepsilon}_o}\right)^{1/n} = \alpha\left(\frac{\dot{a}}{\dot{\varepsilon}c^2 R}\right)^{1/n}, \tag{3}$$

where the constant α is again only a function of the power-law exponent n. Values of c and α for selected values of n were deduced by Bower et al. (1993) from a series of finite element calculations and are listed in Table 1. Eqs. (2) and (3) can be written in terms of an effective stress and effective strain under the indenter. The effective stress σ^{eff} under the indenter is defined as

$$\sigma^{eff} = \frac{F}{\pi a^2}, \tag{4}$$

while the effective strain and strain rate under the indenter are specified as

$$\varepsilon^{eff} = c\sqrt{\frac{h}{2R}}, \tag{5}$$

and

$$\dot{\varepsilon}^{eff} = \frac{\dot{a}}{2R} = c\frac{\dot{h}}{2\sqrt{2hR}}, \tag{6}$$

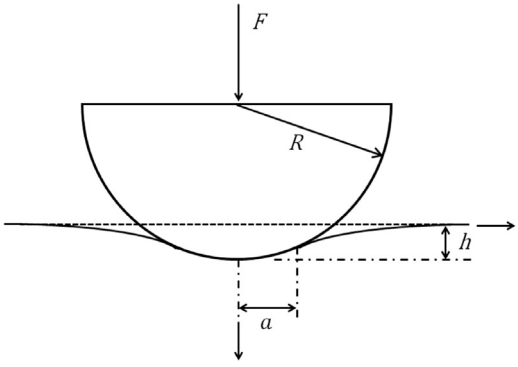

Fig. 1. Schematic diagram of a half-space under indentation by a rigid sphere. The variables F, R, h and a represent the indentation force, indenter radius of curvature, depth of indentation and the radius of permanent indentation, respectively.

Table 1
Indentation model parameters α and c as a function of the power-law exponent n [reproduced from Bower et al. (1993].

n	α	c
1.00	0.849	0.707
1.11	1.085	0.747
1.25	1.332	0.788
1.43	1.602	0.831
1.66	1.886	0.875
2.00	2.176	0.920
2.50	2.465	0.966
3.33	2.734	1.013
5.00	2.973	1.065
10.00	3.110	1.128
100.00	3.051	1.201

respectively. Substituting these definitions in (3) and (4) gives the empirical results of Mulhearn and Tabor (1960):

$$\dot{\varepsilon}^{eff} = \left(\frac{\sigma^{eff}}{\alpha\sigma_o}\right)^n \frac{\dot{\varepsilon}_o c^2}{2}, \tag{7}$$

for the strain rate under an indenter in a solid that undergoes power-law creep.

Dentin is a porous solid. Several models have been proposed in the literature to describe the mechanical behavior of porous and composite materials (see for instance: Jones, 1975; Ji, Gu, & Xia, 2006; Montoya, Arola, & Ossa, 2016). Perhaps the most convenient approach utilizes the rule of mixtures, where the property of interest is estimated according to the sum of contributions from each individual component of the mixture. Following this approach, the effective stress supported by dentin as a function of the lumen area fraction (ξ) (i.e. porosity) can be specified as:

$$\sigma^{eff} = \sigma(1-\xi), \tag{8}$$

where σ^{eff} is the effective stress supported by dentin for a given lumen area fraction (ξ) and σ is the applied stress. The use of this expression assumes that the applied stress applied is supported only by the intertubular and peritubular dentin, and the lumens are considered to have null strength.

3. Experimental study

Human third molars were obtained from selected patients with signed written consent and following all the protocols required and approved by the IRB of the Dentistry Clinic at Universidad Cooperativa de Colombia (UCC), which are in accordance with all the requirements of law. The teeth were obtained from donors living within Medellín, Colombia, between 18 and 25 years of age, and with nearly equal number of males and females. Exclusion criteria included presence of caries and previous restorations. Immediately after extraction, all the specimens were kept in Hank's Balanced Salt Solution (HBSS) at 2 °C to avoid dehydration and loss of mineral (Habelitz, Marshall, Balooch, Marshall, 2002). Furthermore, the specimens were tested within two weeks of extraction to limit the loss of mineral and degradation of the organic materials.

The teeth were sectioned using diamond abrasive slicing equipment with continuous water coolant to obtain specimens from outer (N = 30), middle (N = 35) and inner (N = 27) regions of dentin, which were located approximately at 0.5 mm, 2.0 mm and 3.5 mm away from the DEJ, respectively. The specimens were embedded in cold-cured epoxy resin with the sectioned surface facing outwards as shown in Fig. 2. The exposed dentin was then polished using silicon carbide abrasive paper with successive smaller particle sizes from #600 to #1200 grit. Further polishing was then performed by means of standard red felt polishing cloth wheel and diamond particle suspensions until reaching 3 μm particle size. A detailed explanation of the mounting and polishing process of the samples has been presented in Montoya et al. (2015).

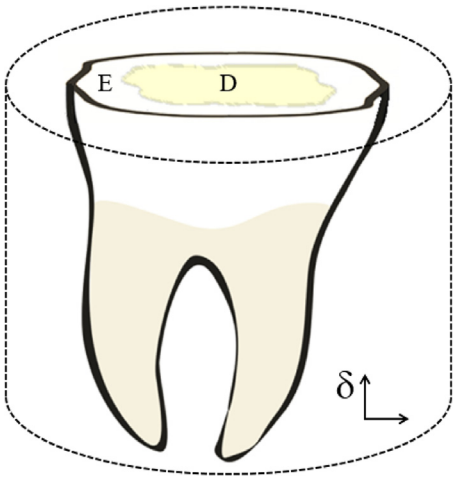

Fig. 2. Schematic diagram of a sectioned molar with exposed dentin that is embedded in cold cured epoxy and ready for the indentation test. The letters D and E refer to dentin and enamel, respectively.

3.1. Spherical indentation tests

Indentation tests were performed using a dedicated fixture with tungsten carbide sphere of 12.67 mm of diameter. This diameter results in a very shallow depth of penetration at low loads, and generates a contact area that is large enough to limit problems associated with local variations in tubule density or other characteristics. As such the variability in microstructure at the specific depths of evaluation are limited. The use of a spherical indenter also generates a homogeneous stress distribution.

Loading was performed using a universal testing machine (Instron Model 3366) equipped with a 500 N load cell and accuracy of 0.1% of full scale. Indentations were made using five different loads (e.g. 1, 5, 10, 30 and 50 N) applied instantaneously and then held constant until reaching steady state deformation behavior (corresponding to approximately 12 h, 2 h, 1 h, 30 min and 15 min, respectively, for each load). Displacement versus time curves were recorded for the duration of the tests. Between 5 and 8 tests were performed for each load and depth of dentin evaluated. The specimens were kept in the HBSS solution during testing to avoid dehydration and minimize friction between the indenter and dentin. A schematic diagram of the test is shown in Fig. 1. The results were evaluated using a one-way ANOVA with a Tukey post-hoc analysis. Significance was defined by $p \leq 0.05$ to establish differences between the groups.

3.2. Chemical composition analysis

A chemical composition analysis of dentin was performed by means of Raman spectroscopy. The measurements were performed at the same locations of the indentation tests in order to find the mineral-to-collagen ratio of dentin at these specific locations. A confocal Raman spectrometer (Horiba Jobin Yvon LabRAM HR) was used and the spectra were obtained over the spectral region of 400 to 1400 cm^{-1}. The Raman spectrometer had a laser diode with a wavelength of 785 nm, with a spot diameter of approximately 1.1 μm. The mineral-to-collagen ratio (χ) was calculated from the ratio of area under the υ_4PO_4 peak at a wavelength of 589 cm^{-1}, which is associated with the phosphate bending of hydroxyapatite, and the area under the amide III peak at

1254 cm^{-1}, which is associated with the collagen amide III band (Goodyear, Gibson, Skakle, Wells, Aspden, 2009; Kazanci, Roschger, Paschalis, Klaushofer, & Fratzl, 2006). These bands were selected for analysis as they are reportedly less susceptible to orientation effects and the polarization direction of the incident light (Kazanci et al., 2006).

3.3. Microstructural analysis

Previous to each indentation test the specimens were used to evaluate the dentin microstructure using optical microscopy (Axiovert 40 MAT, Carl Zeiss Microscopy, NY). The tubule density and diameter were determined from measures obtained at seven unique locations with an approximate window size of 80 μm × 100 μm. In each image, the number of tubules was calculated and expressed as tubules/mm^2. The values from the seven images were averaged and used to determinate the tubule density for each dentin region.

4. Results

4.1. Spherical indentation tests

Fig. 3 shows the evolution of indentation depth (h) within inner dentin as a function of time for selected applied loads. The curves displayed an initial "instantaneous" elastic deformation followed by a decreasing indentation rate (primary or transient creep regime). Thereafter, the response exhibited an approximately constant indentation rate corresponding to the steady-state creep regime. A difference in the elastic deformation was obtained for all indentation loads and in different regions of dentin. The higher values of elastic deformation were found at inner dentin with a decrease as approaching the DEJ. Approximate values of 25 μm were found for middle dentin using an indentation load of 1 N and 125 μm using an indentation load of 50 N. It is worth mentioning that the maximum depth reached from the tests was of around 500 μm, allowing to consider all the tests as being performed on a "half-space", without any substrate effect underneath the indentation.

The indentation rate ($\dot{h}$) was extracted from the steady-state region of each test performed. The distribution in the indentation rate as a function of the load is shown in Fig. 4. There was a significant increase in the indentation rate with load for the three

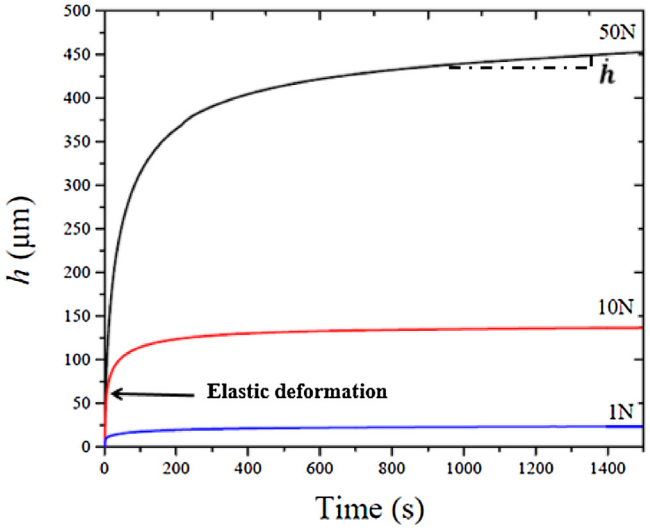

Fig. 3. Selected indentation depth versus time results for inner dentin at applied loads of 1, 10 and 50 N.

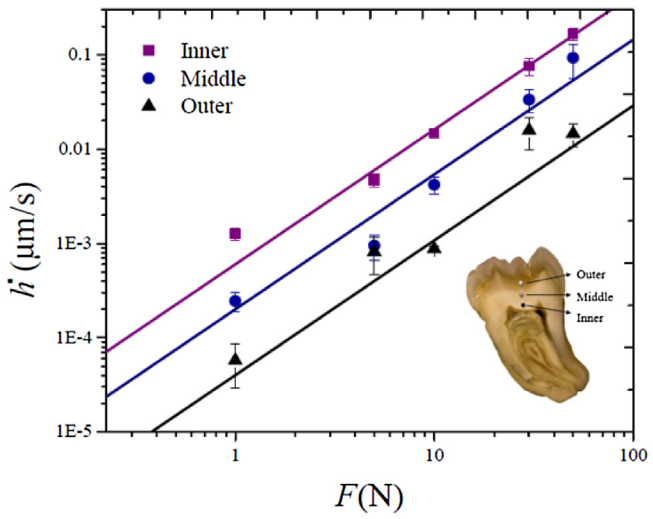

Fig. 4. Steady state indentation rate ($\dot{h}$) versus indentation load for the three regions of dentin evaluated.

different regions evaluated ($p \leq 0.05$). Furthermore, the indentation rates were higher for inner dentin in comparison to results for the middle and outer dentin.

At each of the three depths evaluated the results for indentation creep rate exhibited a power law response that could be described in the form:

$$\dot{h} = \dot{h}_o \left(\frac{F}{F_o}\right)^{n_o}, \tag{9}$$

where $\dot{h}_o$ is a reference indentation rate, F_o is a reference load, F is the applied indentation load and n_o is the power law exponent for dentin. The power law exponent was determined to be constant ($n_o = 1.44$) for all three depths evaluated as estimated through least-squares error evaluation. This response shows that dentin exhibits creep behavior, in which deformation occurs under a constant loads for an extended periods of time; therefore, eqs. (2) to (6) and the model proposed by Bower et al. (1993) can be used to describe the mechanical behavior of dentin.

Results for the effective stress versus effective strain rate calculated from the indentation test results and obtained using Eqs, (4) and (6) are presented in Fig. 5. These results follow a power

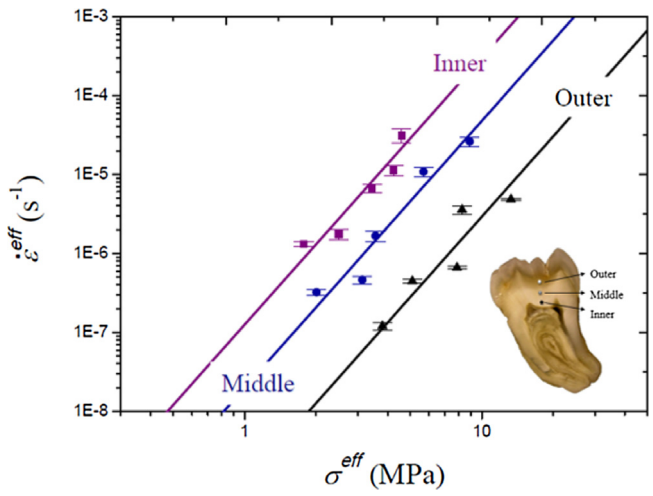

Fig. 5. A comparison of the experimental steady-state effective strain rate plotted in terms of effective stress for coronal dentin (markers) with results from the model (lines).

Table 2
Parameters obtained from coronal dentin for the proposed model.

Parameter	*Value*
n	3.38
α	2.75
c	1.01
σ_o (MPa)	0.50
$\dot{\varepsilon}_o$ (s − 1)	0.013
M	17.02
ϖ	0.48
ξ outer (%)	3.68
ξ middle (%)	6.00
ξ middle (%)	9.28

law behavior with a creep rate exponent of $n = 3.38$. The individual values of the parameters found using Eq. (7) are listed in Table 2. A strong correlation was found between effective stress and effective strain rate for all regions of dentin ($r^2 = 0.90$ for inner, $r^2 = 0.94$ for middle and $r^2 = 0.89$ for outer dentin). The values of σ_o where found to be constant ($\sigma_o = 0.5$ MPa) and not dependent on the region of dentin analyzed. On the other hand, the reference strain rate $\dot{\varepsilon}_o$ was found to exhibit a strong exponential dependence on the mineral to collagen ratio (χ), and an increase with proximity to the pulp (Fig. 6), which corresponds to decreasing mineral content.

A comparison of the values for effective strain rate obtained over the range of applied indentation loads and for the different regions of dentin analyzed is shown in Fig. 7. An increase in effective strain rate occurred with increase in indentation load within each of the three regions. Furthermore, there was a decrease in effective strain rate from inner to outer dentin regions, regardless of the indentation load. Significant differences ($p \leq 0.05$) were observed with increasing distance for most indentation loads as shown in Fig. 7.

4.2. Chemical composition analysis

The mineral-to-collagen ratio (χ) of dentin is shown as a function of the normalized distance from the pulp to the DEJ (ranging from 0 to 1) in Fig. 8. There is an approximate linear increase in mineral-to-collagen ratio approaching the DEJ. A higher mineral to collagen ratio indicates a higher proportion of inorganic material.

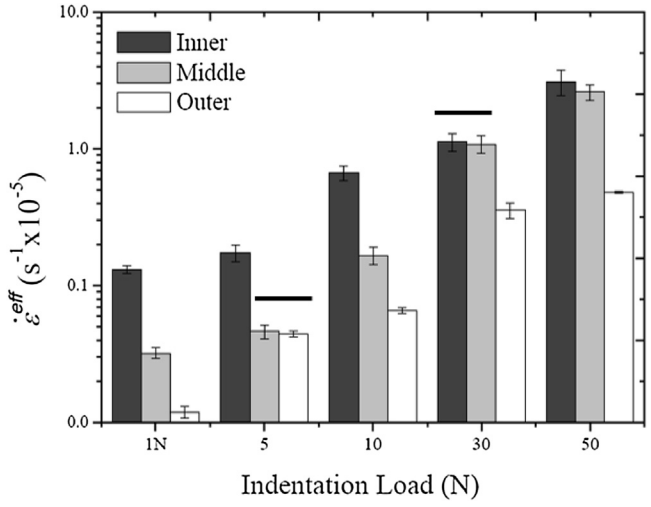

Fig. 7. Effect of indentation load on the effective strain rate for the three different regions of coronal dentin. Columns without significant differences ($p > 0.05$) are grouped with a line.

4.3. Microstructural analysis

Micrographs detailing the microstructure of outer (Fig. 9a), middle (Fig. 9b), and inner (Fig. 9c) dentin are shown for a representative donor tooth in Fig. 9. A highly mineralized peritubular cuff is evident surrounding each dentinal tubule, which is most evident in Fig. 9(a) and (b). As clear from comparison of the micrographs, there is an increase in tubule density and diameter of dentinal tubules as the distance from the DEJ increases. The average density ranged from ~25,000 tubules/mm^2 within the outer dentin to ~35,000 tubules/mm^2 within the inner dentin. Similarly, the average diameter of the tubules ranged from ~1.36 μm at the outer dentin to ~1.81 μm at the inner dentin (Montoya et al., 2015). Based on these measurements there was a significant increase in tubule density and tubule diameter with increasing distance from the DEJ ($p \leq 0.05$).

The results obtained for tubule density and diameter in the three regions of evaluation were used to calculate the lumen area fraction (ξ), which is defined by the ratio between the area occupied by lumens and the total area of dentin measured. The

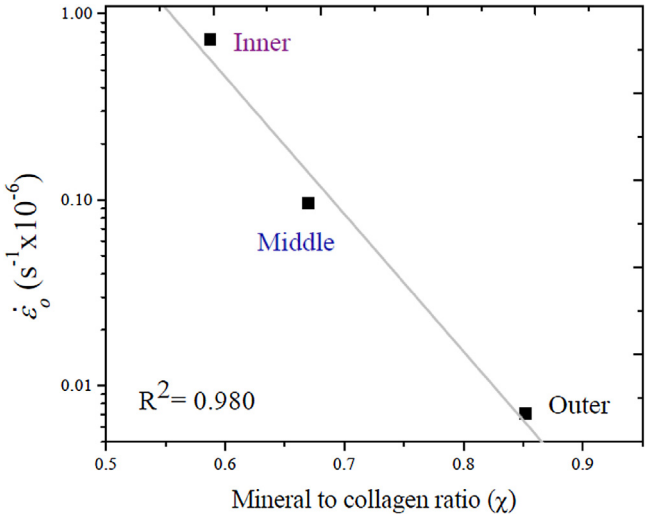

Fig. 6. Dependence of the reference effective strain rate ($\dot{\varepsilon}_o$) on the mineral-to collagen ratio (χ) within the three different regions of coronal dentin.

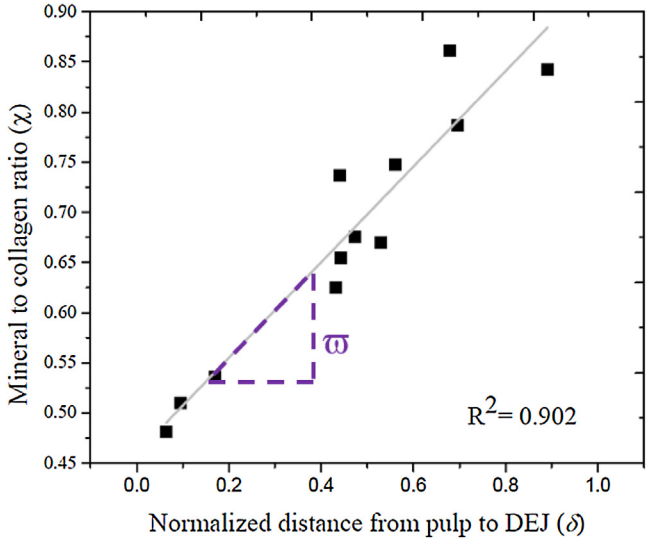

Fig. 8. Distribution of the mineral-to-collagen ratio of dentin according to the normalized distance from the pulp (0) to the DEJ (1).

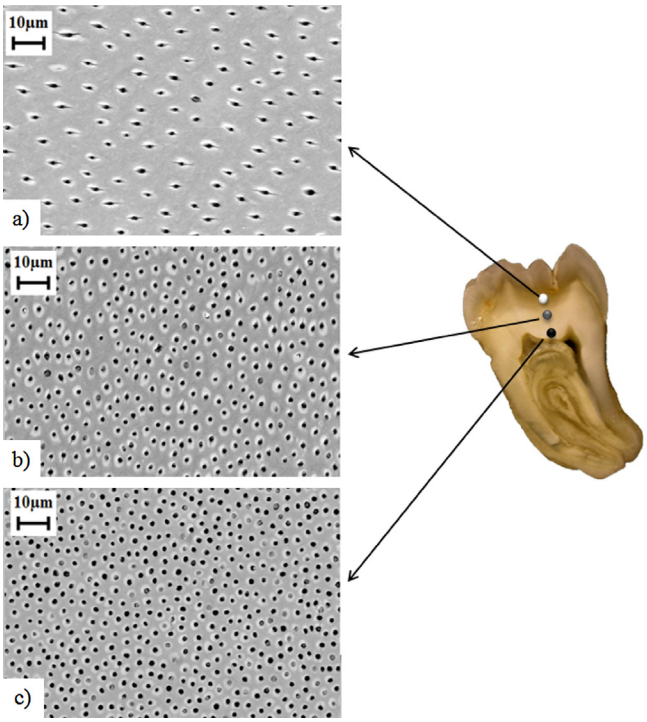

Fig. 9. Micrographs of the representative microstructure within the three regions of evaluation. a) Outer dentin; b) Middle dentin; c) Inner dentin. The results correspond to Montoya et al. (2015).

average lumen area fraction corresponding to the outer and inner regions was $3.68 \pm 0.63\%$ and $9.28 \pm 1.04\%$, respectively. Based on the statistical analysis, there was significant increase ($p \leq 0.05$) in the lumen area fraction as the distance from the DEJ increased.

5. Time dependent deformation model for dentin

A time dependent model is proposed here to capture the steady-state deformation behavior of dentin in response to monotonic loads. The model is motivated by the following experimental observations:

1. The spherical indentation response of dentin was adequately described by a power law model, following the formulation of Bower et al. (1993).
2. The deformation response within dentin was found to be a function of the distance from the pulp to DEJ. Furthermore, this response was found to be affected by spatial variations in the chemical composition (i.e. mineral to collagen ratio) and geometrical factors (i.e. lumen area fraction).

The total strain rate $\dot{\varepsilon}$ of dentin is written as the sum of the elastic $\dot{\varepsilon}^e$ and time dependent (viscous) strain rates $\dot{\varepsilon}^v$. Thus, for an arbitrary loading history, the total strain rate is described by

$$\dot{\varepsilon} = \dot{\varepsilon}^e + \dot{\varepsilon}^v, \tag{10}$$

The elastic response of dentin to an applied load is described by

$$\dot{\varepsilon}^e = \frac{\dot{\sigma}}{E}, \tag{11}$$

where E is the Young's modulus of dentin. The time dependent response can be described using an extension of Eq. (7) as:

$$\dot{\varepsilon}^v = \dot{\varepsilon}^{eff} = \left[\frac{\sigma(1-\xi_i)}{\alpha\sigma_o}\right]^n \frac{\dot{\varepsilon}_{oi} c^2}{2}, \tag{12}$$

where $\dot{\varepsilon}^{eff}$ is the effective strain rate at the normalized position δ_i, σ is the stress resulting from applied load, ξ_i is the lumen area fraction of dentin at position δ_i, n is the creep stress exponent of dentin, c and α are parameters of dentin that depend uniquely on n, $\dot{\varepsilon}_{oi}$ is a reference effective strain rate at position δ_i and σ_o is the reference stress for dentin.

The effective strain rate $\dot{\varepsilon}_{oi}$ at position δ_i is dependent on the chemical composition and can be calculated according to:

$$\dot{\varepsilon}_{oi} = \dot{\varepsilon}_o e^{-M\delta_i \varpi}, \tag{13}$$

where $\dot{\varepsilon}_o$ is the reference effective strain rate of a "reference" dentin with the lowest degree of mineral content (e.g. with no mineral), ϖ is the spatial trend in chemical composition of dentin, which is described by the slope of the change of mineral-to-collagen ratio (χ) with the normalized distance from pulp to DEJ (δ), as shown in Fig. 8; δ is the normalized position and M is the mineralization rate decay of dentin. This parameter describes the spatial variations in mineralization of dentin. The importance of M to the decay in reference strain rate is shown schematically in Fig. 10. Note that a large value of M corresponds to a dentin with larger gradient in $\dot{\varepsilon}_o$ from the pulp to the DEJ, and vice versa.

To obtain the strain resulting from an applied stress history it is then necessary to integrate Eqs. (10) to (12) with respect to time. The model was then used to describe the time dependent behavior of dentin using the parameters listed in Table 2 in the three normalized positions of $\delta = 0.25$ (for inner dentin), $\delta = 0.55$ (for middle dentin) and $\delta = 0.85$ (for outer dentin). These results for the model are added in Fig. 5. As evident from the comparison of model and experiment, there is good agreement for all three regions of dentin evaluated.

6. Approximate calibration of the model

Six parameters – ξ, n, $\dot{\varepsilon}_{oi}$, σ_o, ϖ and M – are required in the proposed model to fully describe the effective strain rate of coronal dentin within the specific spatial location. A four-step approximate calibration procedure is described below and requires a minimum of four spherical indentations and two dentin depths.

Step 1: The first step is to characterize the steady-state spherical indentation behavior of dentin at a specific depth of

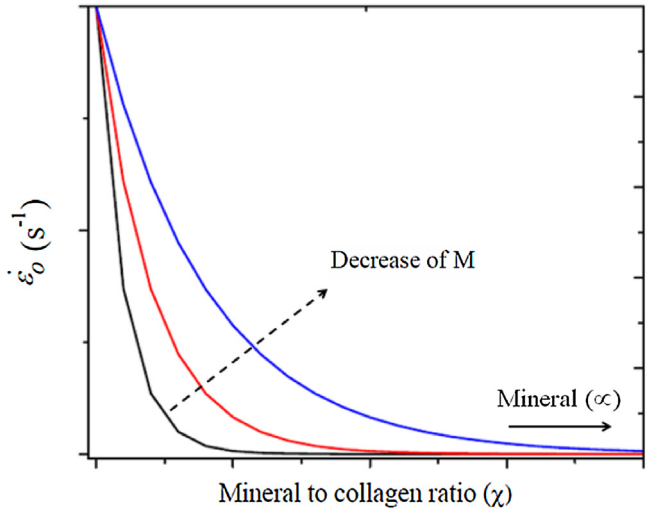

Fig. 10. Schematic diagram showing how changes in the degree of mineralization affect the response of the reference strain rate $\dot{\varepsilon}_o$. This plot is presented without numerical data intentionally to convey the trend and importance of the parameters.

interest δ_1. Experience indicates that it is adequate to perform two spherical indentation tests at two given constant loads (e.g.: $F_1 = 10$ N, $F_2 = 40$N). From those two tests results the steady-state indentation rates $\dot{h}_1$ and $\dot{h}_2$ are estimated, respectively. Equation (9) can be used to obtain n_o according to:

$$n_o = \frac{log(\dot{h}_1/\dot{h}_2)}{log(F_1/F_2)}. \quad (14)$$

The parameters α and c can be obtained directly from Table 1. Now using equations (4) and (6), it is possible to calculate $\dot{\varepsilon}_i^{eff}$ and σ_i^{eff} for each of the tests performed, and n is calculated using:

$$n = \frac{log\left(\dot{\varepsilon}_1^{eff}/\dot{\varepsilon}_2^{eff}\right)}{log\left(\sigma_1^{eff}/\sigma_2^{eff}\right)}, \quad (15)$$

and calculate the new values of α and c. The reference stress σ_o can be assumed constant with a value of 0.5 MPa. Thereafter, $\dot{\varepsilon}_{o1}$ can be found for the first depth according to

$$\dot{\varepsilon}_{o1} = \dot{\varepsilon}_1^{eff}\left(\frac{\sigma_1^{eff}}{\sigma_o}\right)^{1/n}. \quad (16)$$

Step 2: Repeat Step 1 for a different depth to obtain $\dot{\varepsilon}_{o2}$.

Step 3: At each of the depths tested, measure the lumen area fractions (ξ_1 and ξ_2) and mineral-collagen ratios (χ_1 and χ_2). The spatial trend in chemical composition ϖ can be found from:

$$\varpi = \frac{\chi_2 - \chi_1}{\delta_2 - \delta_1}. \quad (17)$$

Step 4: The mineral rate decay M can be estimated according to:

$$M = \frac{1}{\varpi(\delta_2 - \delta_1)} ln\left(\frac{\dot{\varepsilon}_{o2}}{\dot{\varepsilon}_{o1}}\right). \quad (18)$$

Thus, a minimum of two depths with four spherical indentation tests are necessary to calibrate the model proposed. Of course, more tests and depths can be conducted to improve the statistical accuracy of the fitted parameters.

7. Discussion

The creep behavior of coronal dentin was studied using spherical indentation, and the results supported the development of a model describing the time dependent response as a function of spatial variations of the dentinal tubules density (lumen area fraction) and chemical composition (mineral-to-collagen ratio). The relationship between effective stress and effective strain rate showed that dentin exhibits a non-linear creep behavior with a stress exponent of $n = 3.38$, which is indicative of a non-linear viscous solid.

The power-law behavior of hard tissues has been previously reported in the literature. Fig. 11 shows a comparison of the results obtained for the steady state creep rate for coronal dentin and published data for compact bovine bone (in uniaxial tension, Rimnac, Petko, Santner, Wright, 1993) and radicular dentin (in uniaxial compression Jantarat, Palamara, Lindner, & Messer, 2002). The results reported by these authors were used to calculate the parameters of the power law creep model (Eq. (1)) shown in Table 3.

The creep stress exponents found for compact bovine bone ($n = 5.2$) and radicular dentin ($n = 1.5$) are in general agreement with that estimated here for coronal dentin. Based on the creep exponents, coronal dentin (e.g. this study) and compact bovine bone exhibit more extensive non-linear behavior than radicular dentin. This behavior could be attributed to the creep characteristics of the type I collagen present in both materials. While type I collagen is the primary organic component of both tissues, the hydroxylysine content is higher in dentin than in bone (Kumar, 2010). Hydroxylysine content has been connected with covalent cross-linking of the collagen chains and manifests as an increase in the stiffness and strength of collagen (Cardinale, Newton, & Nosaka, 2011). This difference in collagen conformation could explain, in part, why compact bone exhibits higher non-linear behavior than dentin. Conversely, radicular dentin displays a value of stress exponent closer to true linear viscoelastic behavior ($n = 1$). The difference in viscous response between coronal and radicular dentin could be associated with differences in the dentinal tubule orientation relative to the applied stress. In compression of radicular dentin the tubules are oriented perpendicular to the stress direction. In addition, radicular dentin has higher tubule density and smaller lumens in comparison to those qualities of the crown (Arola et al., 2009), which could contribute to larger volume fraction of peritubular dentin without collagen fibrils (Xu & Wang, 2012). These qualities could be responsible for the lower degree of time dependent deformation in radicular dentin.

From the results obtained from both the model and experimental data, the inner dentin exhibited the highest effective strain rate ($\dot{\varepsilon}^{eff}$), and there was a decrease approaching the DEJ. This

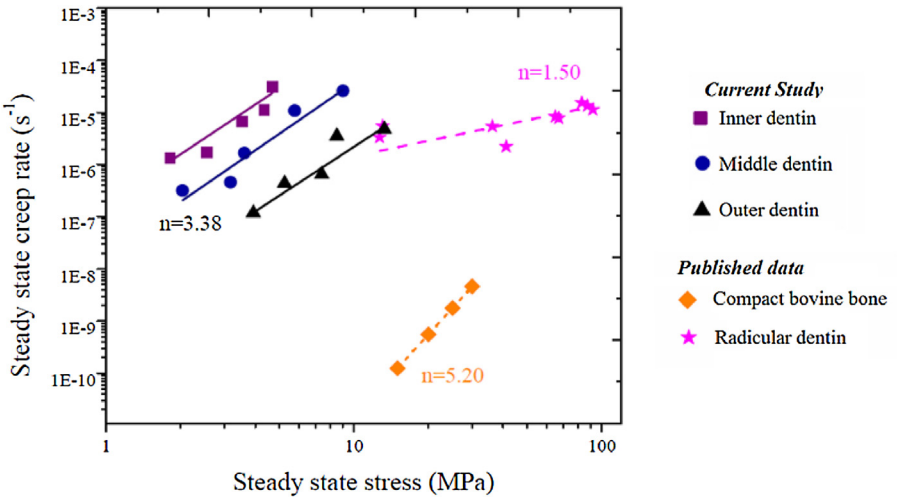

Fig. 11. A comparison of experimental results reported for the steady state creep rate of compact bovine bone (Rimnac et al., 1993) and radicular dentin (Jantarat et al., 2002) with results of the current study for human coronal dentin.

Table 3
A comparison of the parameters describing the basic power-law creep behavior reported in the literature for different hard tissues. The results for coronal dentin were developed in the present investigation.

Parameter	*Compact bovine bone* (Rimnac et al., 1993)	*Radicular dentin* (Jantarat et al., 2002)	*Coronal Dentin*
n	5.20	1.47	3.38
σ_o (MPa)	0.50	0.50	0.50
$\dot{\varepsilon}_o$ $(s-1)$	4.21×10^{-15}	7.00×10^{-9}	Outer: 7.07×10^{-9} Middle: 9.63×10^{-8} Inner: 7.31×10^{-7}

behavior is related to the composition and mineralization pattern during dentinogenesis. In the course of odontogenesis, odontoblasts produce primary dentin until eruption of the tooth (Schour, 1948). As soon as the tooth erupts, the formation of secondary dentin begins and continues throughout life (Goldberg, Kulkarni, Young, & Boskey, 2011). Prior to mineralization of dentin, an extracellular organic matrix is produced (Almushayt, Narayanan, Zaki, George, 2006), making the dentin located nearest the pulp (newly produced by odontoblasts) to display the lowest degree of mineralization, leading to higher strain rates than for the subsequent dentin layers. Furthermore, the larger tubule diameters of inner dentin provide a larger volume of "free spaces" occupied by dentinal fluid during normal function of the tooth. This fluid has been reported to have a similar composition to plasma (e.g.: 90–92% water and the remaining corresponding to solids) (Chatterjea & Shinde, 2012; Driessens & Verbeeck, 1990). The water has been suggested to have a plasticizing effect in dentin, participating in its viscoelastic behavior (Jameson, Hood, & Tidmarsh, 1993; Kishen & Asundi, 2005).

Although results from the current study provide further understanding of the time dependent deformation behavior of human dentin, there are recognized limitations that should be considered. There has been a good deal of discrepancy concerning the distribution in mineral to collagen ratio of coronal dentin. Some researchers have found that the amount of mineral content increases from the pulp to the DEJ (Hayakawa et al., 2000; Angker, Nockolds, Swain, & Kilpatrick, 2004; Clementino-Luedemann and Kunzelmann, 2006; Montoya et al., 2015), while others have reported the opposite trend, namely a reduction in this direction (e.g. Ryou et al., 2011; Xu et al., 2009). This contradiction would not require changes to the proposed model since a higher mineral-to-collagen ratio (higher mineral content) in any position of dentin will be accounted for directly by the term $\delta_i \varpi$ in Eq. (13). However, if the model is applied to the dentin of seniors, then some adjustments may needed to account for the changes in microstructure, as well as for the potential effects of collagen cross-linking (Ivancik, Majd, Bajaj, Romberg, & Arola, 2012; Miura et al., 2014).

It is worth noting here that the model in its present form can be applied only to coronal dentin and wherein the indentation load is applied parallel to the dentinal tubules. If the direction of the indentation load is changed, a correction factor must be considered, corresponding to the stress concentration posed by the dentinal tubules. These factors are commonly used in the study of mechanical properties of porous materials (Balshin, 1949; Boccaccini, Ondracek, & Mombello, 1996) and even to predict the fracture toughness of dentin (Montoya et al., 2016). A correction of the stress concentration factor is expected to be important if grinding or clenching problems are investigated, where shear forces are deemed to be critical.

It is also worth noting that it has been reported that dentinal tubules possess sigmoid "S" shape distribution in coronal dentin, as shown schematically in Fig. 12a (Gomez de Ferraris & Muñoz, 2009; Nanci, 2008). This sigmoid shape has been known to have an important effect on the mechanical response of dentin. Based on this quality, when a load is applied, the dentinal tubules have different orientations (i.e. angles) relative to the direction of the load, increasing the potential for the tissue to exhibit anisotropy. This behavior was analyzed by Han et al. (2012), who developed a model to evaluate the mechanical response of the tubules depending on their angles. However, the time dependent model proposed here assumes that dentinal tubules extend straight from the pulp up to the DEJ and that the three regions of dentin analyzed (outer, middle, and inner) are homogenous and isotropic. It is then expected that the sigmoid shape might have an effect on the model results depending on the specific orientation of the tubules. For

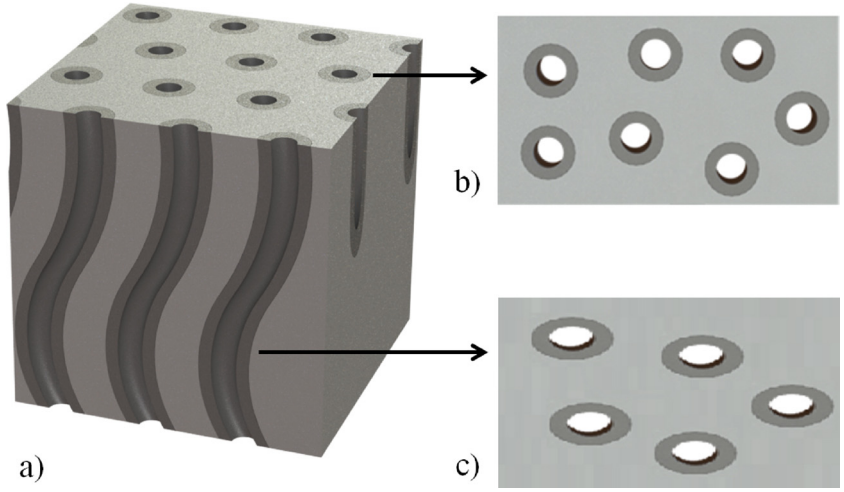

Fig. 12. Schematic representation of how the tubules are distributed in coronal dentin. The s-shaped curvature is shown, which influences the relative tubule orientation and shape, depending on the relative location of analysis.

instance, if the dentinal area described by the model corresponds to straight areas of the tubules (Fig. 12b), the model results will be unaffected. On the other hand, if the description corresponds to wavy regions of the lumens (Fig. 12c), some discrepancy between model and reality could be expected. An analysis of the error associated with these geometrical factors and other well-known characteristics of dentin, like branching of dentinal tubules and change of the diameter of peritubular dentin with depth, are beyond the scope of this study and is a topic reserved for future study.

8. Conclusions

The time dependent deformation behavior of coronal dentin was studied using instrumented spherical indentation. The experimental results showed that the deformation behavior followed a power law behavior, which was appropriately captured by an extension to previously proposed models for the time dependent deformation behavior of structural materials. The model accounts for the spatial variations of chemical composition (e.g. mineral to collagen ratio) and microstructure (e.g. tubule density) of coronal dentin. Regions with higher mineral to collagen ratio exhibited a stiffening effect, with reduced strain rate for indentation loads. Similarly, a reduction in tubule density also caused a decrease in the deformation behavior. The power law creep exponent for dentin was found to have a value of $n = 3.38$ which was independent of the spatial variations in composition and microstructure. Furthermore, this parameter was found to be dependent on the specific composition of the collagen present in the tissue and not on its amount.

Conflict of interests

I affirm that I have no financial affiliation (e.g., employment, direct payment, stock holdings, retainers, consultantships, patent licensing arrangements or honoraria), or involvement with any commercial organization with direct financial interest in the subject or materials discussed in this manuscript, nor have any such arrangements existed in the past. Furthermore, we have no conflict of interests to declare for this study.

Funding

Partial funding of this research was granted by Departamento Administrativo de Ciencia, Tecnología e Innovación, Colciencias for Ms. C. Montoya PhD studies.

Ethical approval

Testing samples were obtained from selected patients after written consent and following all the protocols required by the Dental Clinic at Universidad Cooperativa de Colombia (UCC).

Acknowledgements

The authors would like to express their gratitude to Prof. Santiago Arango and Prof. Alejandro Peláez from the Dental Clinic of Universidad Cooperativa de Colombia for providing teeth for this study and to Departamento Administrativo de Ciencia, Tecnología e Innovación, Colciencias for the Ph.D. Grant to Mrs. C. Montoya.

References

Ahearne, M., Yang, Y., Then, K. Y., & Liu, K. K. (2007). An indentation technique to characterize the mechanical and viscoelastic properties of human and porcine corneas. *Annals of Biomedical Engineering*, *35*(9), 1608–1616.

Alfrey, T., & Doty, P. (1945). The methods of specifying the properties of viscoelastic materials. *Journal of Applied Physics*, *16*(11), 700–713.

Almushayt, A., Narayanan, K., Zaki, A. E., & George, A. (2006). Dentin matrix protein 1 induces cytodifferentiation of dental pulp stem cells into odontoblasts. *Gene Therapy*, *13*(7), 611–620.

Angker, L., Nockolds, C., Swain, M. V., & Kilpatrick, N. (2004). Quantitative analysis of the mineral content of sound and carious primary dentine using BSE imaging. *Archives of Oral Biology*, *49*(2), 99–107.

Arola, D., Ivancik, J., Majd, H., Fouad, A., Bajaj, D., Zhang, X. Y., et al. (2009). Microstructure and mechanical behavior of radicular and coronal dentin. *Endodontic Topics*, *20*(1), 30–51.

Balshin, M. (1949). Relation of mechanical properties of powder metals and their porosity and the ultimate properties of porous-metal ceramic materials. *Dokl Askd SSSR*, *67*, 831–834.

Bertassoni, L. E., Kury, M., Rathsam, C., Little, C. B., & Swain, M. V. (2015). The role of proteoglycans in the nanoindentation creep behavior of human dentin. *Journal of the Mechanical Behavior of Biomedical Materials*, *55*, 264–270.

Boccaccini, A. R., Ondracek, G., & Mombello, E. (1996). Determination of stress concentration factors in porous materials. *Journal of Materials Science Letters*, *15*(6), 534–536.

Bower, A. F., Fleck, N. A., Needleman, A., & Ogbonna, N. (1993). Indentation of a power law creeping solid. *Proceedings of the Royal Society of London A*, *441*(1911), 97–124.

Cardinale, M., Newton, R., & Nosaka, K. (Eds.). (2011). *Strength and conditioning: Biological principles and practical applications*. John Wiley & Sons.

Chatterjea, M. N., & Shinde, R. (2012). *Textbook of medical biochemistry*, eigth ed. New Delhi: Jaypee Brothers.

Cheneler, D., Mehrban, N., & Bowen, J. (2013). Spherical indentation analysis of stress relaxation for thin film viscoelastic materials. *Rheologica Acta*, *52*(7), 695–706.

Chuang, S. F., Lin, S. Y., Wei, P. J., Han, C. F., Lin, J. F., & Chang, H. C. (2015). Characterization of the elastic and viscoelastic properties of dentin by a nanoindentation creep test. *Journal of Biomechanics*, *48*(10), 2155–2161.

Clementino-Luedemann, T. N. R., & Kunzelmann, K. H. (2006). Mineral concentration of natural human teeth by a commercial micro-CT. *Dental Materials Journal*, *25*(1), 113–119.

Deymier-Black, A. C., Yuan, F., Singhal, A., Almer, J. D., Brinson, L. C., & Dunand, D. C. (2012). Evolution of load transfer between hydroxyapatite and collagen during creep deformation of bone. *Acta Biomaterialia*, *8*(1), 253–261.

Driessens, F. C., & Verbeeck, R. K. (1990). *Biominerals*. CRC Press.

Duncanson, M. G., & Korostoff, E. (1975). Compressive viscoelastic properties of human dentin: I. Stress-relaxation behavior. *Journal of Dental Research*, *54*(6), 1207–1212.

Goldberg, M., Kulkarni, A. B., Young, M., & Boskey, A. (2011). Dentin: Structure, Composition and Mineralization: The role of dentin ECM in dentin formation and mineralization. *Front Biosci (Elite Ed)*, *3*, 711–735.

Gomez de Ferraris, M. E. G., & Muñoz, A. C. (2009). *Histologa, embriologa e ingeniera tisular bucodental/Histology, embryology and oral tissue engineering*. Ed. Médica Panamericana.

Goodyear, S. R., Gibson, I. R., Skakle, J. M., Wells, R. P., & Aspden, R. M. (2009). A comparison of cortical and trabecular bone from C57 Black 6 mice using Raman spectroscopy. *Bone*, *44*(5), 899–907.

Graham, G. A. (1965). The contact problem in the linear theory of viscoelasticity. *International Journal of Engineering Science*, *3*(1), 27–46.

Habelitz, S., Marshall, G. W., Balooch, M., & Marshall, S. J. (2002). Nanoindentation and storage of teeth. *Journal of Biomechanics*, *35*(7), 995–998.

Han, C. F., Wu, B. H., Chung, C. J., Chuang, S. F., Li, W. L., & Lin, J. F. (2012). Stress–strain analysis for evaluating the effect of the orientation of dentin tubules on their mechanical properties and deformation behavior. *Journal of the Mechanical Behavior of Biomedical Materials*, *12*, 1–8.

Hayakawa, T., Mishima, H., Yokota, I., Sakae, T., Kozawa, Y., & Nemoto, K. (2000). Application of high resolution microfocus X-ray CT for the observation of human tooth. *Dental Materials Journal*, *19*(1), 87–95.

Hill, R. F. R. S., Storakers, B., & Zdunek, A. B. (1989). A theoretical study of the Brinell hardness test. *Proceedings of the Royal Society of London A*, *423*(June (1865)), 301–330.

Hunter, S. C. (1960). The Hertz problem for a rigid spherical indenter and a viscoelastic half-space. *Journal of the Mechanics and Physics of Solids*, *8*(4), 219–234.

Ivancik, J., Majd, H., Bajaj, D., Romberg, E., & Arola, D. (2012). Contributions of aging to the fatigue crack growth resistance of human dentin. *Acta Biomaterialia*, *8*(7), 2737–2746.

Jafarzadeh, T., Erfan, M., & Watts, D. C. (2004). Creep and viscoelastic behaviour of human dentin. *JDT*, *1*(1), 5–14.

Jameson, M. W., Hood, J. A. A., & Tidmarsh, B. G. (1993). The effects of dehydration and rehydration on some mechanical properties of human dentine. *Journal of Biomechanics*, *26*(9), 1055–1065.

Jantarat, J., Palamara, J. E., Lindner, C., & Messer, H. H. (2002). Time-dependent properties of human root dentin. *Dental Materials*, *18*(6), 486–493.

Ji, S., Gu, Q., & Xia, B. (2006). Porosity dependence of mechanical properties of solid materials. *Journal of Materials Science*, *41*(6), 1757–1768.

Jones, R. M. (1975). *Mechanics of composite materials*, 2nd ed. Washington D.C: Scripta Book Company.

Kazanci, M., Roschger, P., Paschalis, E. P., Klaushofer, K., & Fratzl, P. (2006). Bone osteonal tissues by Raman spectral mapping: Orientation–composition. *Journal of Structural Biology*, *156*(3), 489–496.

Kim, J. H. (2008). *Analysis of surface layer effects in spherical contact*. ProQuest.
Kinney, J. H., Marshall, S. J., & Marshall, G. W. (2003). The mechanical properties of human dentin: A critical review and re-evaluation of the dental literature. *Critical Reviews in Oral Biology and Medicine*, *14*(1), 13–29.
Kishen, A., & Asundi, A. (2005). Experimental investigation on the role of water in the mechanical behavior of structural dentine. *Journal of Biomedical Materials Research Part A*, *73*(2), 192–200.
Korostoff, E., Pollack, S. R., & Duncanson, M. G. (1975). Viscoelastic properties of human dentin. *Journal of Dental Research*, *9*(6), 661–674.
Kumar, C. S. (2010). *Biomimetic and bioinspired nanomaterials*, *Vol. 3*, Weinheim: John Wiley & Sons.
Lee, E. H., & Radok, J. R. M. (1960). The contact problem for viscoelastic bodies. *Journal of Applied Mechanics*, *27*(3), 438–444.
Miura, J., Nishikawa, K., Kubo, M., Fukushima, S., Hashimoto, M., Takeshige, F., et al. (2014). Accumulation of advanced glycation end-products in human dentine. *Archives of Oral Biology*, *59*(2), 119–124.
Montoya, C., Arango-Santander, S., Peláez-Vargas, A., Arola, D., & Ossa, E. A. (2015). Effect of aging on the microstructure, hardness and chemical composition of dentin. *Archives of Oral Biology*, *60*(12), 1811–1820.
Montoya, C., Arola, D., & Ossa, E. A. (2016). Importance of tubule density to the fracture toughness of dentin. *Archives of Oral Biology*, *67*, 9–14.
Mulhearn, T. O., & Tabor, D. (1960). Creep and Hardness of metals: A physical study. *Journal of the Institute of Metals*, *89*, 7–12.
Nanci, A. (2008). *Ten cate's oral histology: Development, structure, and function*. 7th ed. St. Louis, MO: Mosby.
Pashley, D., Okabe, A., & Parham, P. (1985). The relationship between dentin microhardness and tubule density. *Endodontics and Dental Traumatology*, *1*(5), 176–179.
Rimnac, C. M., Petko, A. A., Santner, T. J., & Wright, T. M. (1993). The effect of temperature, stress and microstructure on the creep of compact bovine bone. *Journal of Biomechanics*, *26*(3), 219–228.
Ryou, H., Amin, N., Ross, A., Eidelman, N., Wang, D. H., Romberg, E., et al. (2011). Contributions of microstructure and chemical composition to the mechanical properties of dentin. *Journal of Materials Science*, *22*(5), 1127–1135.
Ryou, H., Romberg, E., Pashley, D. H., Tay, F. R., & Arola, D. (2012). Nanoscopic dynamic mechanical properties of intertubular and peritubular dentin. *Journal of the Mechanical Behavior of Biomedical Materials*, *7*, 3–16.
Schour, I. (1948). Development and growth of teeth. *Oral Surgery, Oral Medicine, Oral Pathology*, *1*(4), 346–354.
Shen, Z. L., Kahn, H., Ballarini, R., & Eppell, S. J. (2011). Viscoelastic properties of isolated collagen fibrils. *Biophysical Journal*, *100*(12), 3008–3015.
Staines, M., Robinson, W. H., & Hood, J. A. A. (1981). Spherical indentation of tooth enamel. *Journal of Materials Science*, *16*(9), 2551–2556.
Tesch, W., Eidelman, N., Roschger, P., Goldenberg, F., Klaushofer, K., & Fratzl, P. (2001). Graded microstructure and mechanical properties of human crown dentin. *Calcified Tissue International*, *69*(3), 147–157.
Trengrove, H. G., Carter, G. M., & Hood, J. A. (1995). Stress relaxation properties of human dentin. *Dental Mater*, *11*(5), 305–310.
Xu, C., & Wang, Y. (2012). Chemical composition and structure of peritubular and intertubular human dentine revisited. *Archives of Oral Biology*, *57*(4), 383–391.
Xu, C., Yao, X., Walker, M. P., & Wang, Y. (2009). Chemical/molecular structure of the dentin–enamel junction is dependent on the intratooth location. *Calcified Tissue International*, *84*(3), 221–228.